

Computer-Aided Small-Signal Analysis Based on Impulse Response of DC/DC Switching Power Converters

Dragan Maksimović, *Member, IEEE*

Abstract—The paper describes a method for automated small-signal frequency response analysis based on transient response obtained using a general-purpose simulation tool such as simulation program with integrated circuit emphasis (SPICE). The method is based on using the simulation tool to evaluate the converter impulse response. The main advantage of the proposed method as a design verification tool is that frequency responses can be generated efficiently for any converter configuration and any model complexity supported by the general-purpose simulator. Application examples are included to demonstrate very good correlation between the generated responses and experimental data, and to compare the results with predictions of approximate analytical methods. In particular, the method is applied to investigate high-frequency dynamics of pulse width modulation (PWM) converters operating in discontinuous conduction mode, and the results are used to compare and validate several existing analytical modeling approaches.

Index Terms—DC–DC power conversion, discontinuous conduction mode, modeling of pulse width modulated power converters, small-signal analysis.

I. INTRODUCTION

NUMEROUS analytical techniques have been developed for small-signal, frequency-domain analysis of power electronic systems, including approximate continuous-time (averaged) and sampled-data models, which are now well described in textbooks [1]–[3], as well as more accurate and general but more complex models (such as [4], [5], [7]). In practice, however, there are often configurations, control methods, or operating modes where appropriate small-signal models are not available or are difficult to derive. In these cases, and also for general design verification where effects of parasitics, snubbers, auxiliary circuits for soft switching etc, are considered, computer-aided analysis tools are indispensable. This paper describes an automated method to obtain system control-to-output frequency responses using a general-purpose time-domain simulation tool (such as PSPICE) or any other SPICE derivative) for any circuit configuration supported by the simulator. The approach to finding system frequency responses via time-domain responses generated by a general-purpose simulator was reported in [6]. The method described in [6] was based on a basic sampled-data model which may fail to predict observed responses in some cases. An automated small-signal frequency-domain analyzer was described in [8] based on an

algorithm similar to the algorithms presented in [4], [5], [7]. In this algorithm, steady-state time-domain solution (named “small-signal steady-state”) is found for the case when inputs have one or more small-signal sinusoidal sources on top of the large-signal, steady-state waveforms. However, the algorithm was based on the assumption that the system can be modeled as piecewise linear, and the implementation was tied to a special-purpose switched-circuit simulator. In [9], small-signal transfer functions of switching converters were obtained using system identification techniques. A pseudorandom perturbation signal with the spectrum spanning the entire range of frequencies of interest is added to an input. The system is then simulated in time domain using a general-purpose simulator to generate output responses. Finally, the simulation results are used as inputs to the identification algorithm to determine parameters in a small-signal model of selected order. The approach does meet our objectives of obtaining frequency responses using results from a time-domain general-purpose simulator, but is empirical in nature, and may require experimenting with the assumed system order, perturbation signal or length of simulation.

The small-signal control-to-output frequency response of a dc/dc switch-mode power converter is usually obtained by driving a control input with a small-amplitude voltage source of angular frequency ω on top of a dc bias. The components of converter voltages or currents at the signal-injection frequency ω are then measured through a band-pass filter centered at ω . By sweeping the signal-injection frequency, magnitude and phase responses are then obtained as functions of frequency. This measurement process implicitly assumes that the converter can be considered linear, time-invariant system if the signal amplitudes are sufficiently small. This assumption is made in all analytical techniques developed over the years for small-signal analysis of switching power converters.

The most popular, averaging techniques, result in continuous-time, large-signal, nonlinear models. From these models, standard perturbation and linearization techniques lead to linear, time-invariant, small-signal models that can in most cases successfully predict converter frequency responses at least at frequencies sufficiently smaller than the switching frequency. It has been shown that models that recognize sampled-data nature of switching converters can extend the range of frequencies where model predictions match measurement results. In some cases, most notably in modeling converters with current-mode programming, continuous-time models have been successfully enhanced to include predictions of sampled-data effects, such as subharmonic oscillations. In recent years, analytical models that can, in principle,

Manuscript received July 29, 1998; revised August 14, 2000. This work was supported by the National Science Foundation under Grant ECS-9703449. Recommended by Associate Editor T. Sloane.

The author is with the Department of Electrical and Computer Engineering, University of Colorado, Boulder, CO 80309-0425 USA.

Publisher Item Identifier S 0885-8993(00)09809-4.

match measurement results exactly (and at all frequencies) have been developed [4], [5], [7]. All of these analytical models rely on the simplifying assumption that switching converters can be modeled as switched piecewise-linear systems. Furthermore, since these most general and theoretically most accurate methods most often yield analytical results that offer very little insight, it appears that such methods are well suited mainly for design verification purposes via computer-implemented tools.

In this paper, we approach the problem of finding converter small-signal frequency responses with two objectives: 1) to obtain results that can match measurement results in general, and at all relevant frequencies and 2) to facilitate practical implementation of the small-signal analysis using a general-purpose time-domain simulation tool. With these objectives in mind we start from a fundamental relation between time-domain and frequency-domain responses: in a linear, time-invariant system, a system transfer function is the Laplace transform of the system impulse response, i.e., the Laplace transform of the system transient response obtained when the input is excited by a delta function. One could therefore obtain a system transfer function by running transient simulation for sufficiently long time, and by evaluating the Laplace transform of the transient response. In this paper, we show that this approach can be implemented without the need to generate and process the impulse response over a very long time interval.

The approach to finding the converter small-signal frequency-domain responses via evaluation of the system impulse response in time domain is first introduced in Section II using a simple pulse width modulation (PWM) converter example operating in discontinuous conduction mode (DCM). Section III gives a general formulation of the method. Practical implementation of the method using a general-purpose simulator is described in Section IV. Application examples are given in Section V.

II. CASE STUDY: HIGH-FREQUENCY DYNAMICS OF PWM CONVERTERS OPERATING IN DISCONTINUOUS CONDUCTION MODE

In this section, we introduce the impulse-response based analysis method using a PWM converter operating in DCM. This example is then used to evaluate and compare several existing analytical approaches to modeling PWM converters in DCM.

Consider the simple inductor-only boost converter in Fig. 1. Both input and output are constant dc voltage sources, and the converter is operated in DCM, with typical converter waveforms shown in Fig. 1. The control input is the length of the switch on-time, i.e., the switch duty ratio d . The output is the inductor current i_L . This example is constructed so that we can examine *only* the high-frequency effects due to the inductor dynamics.

To obtain the system impulse response, the switch duty ratio d is perturbed to $D+\hat{d}$ only at the initial sample instant, at $t=0$. Since the converter operates in DCM, the resulting output perturbation \hat{i}_L reduces to 0 and stays 0 for $t > D_2T$. As a result, the Laplace transform of the output can be evaluated easily

$$\begin{aligned} \hat{i}_L(s) &= \mathcal{L}[\hat{i}_L(t)] = \int_0^\infty \hat{i}_L(t)e^{-st} dt = \Delta i \int_0^{D_2T} e^{-st} dt \\ &= \frac{V_o}{L} \hat{d}T \frac{1 - e^{-sD_2T}}{s}. \end{aligned} \quad (1)$$

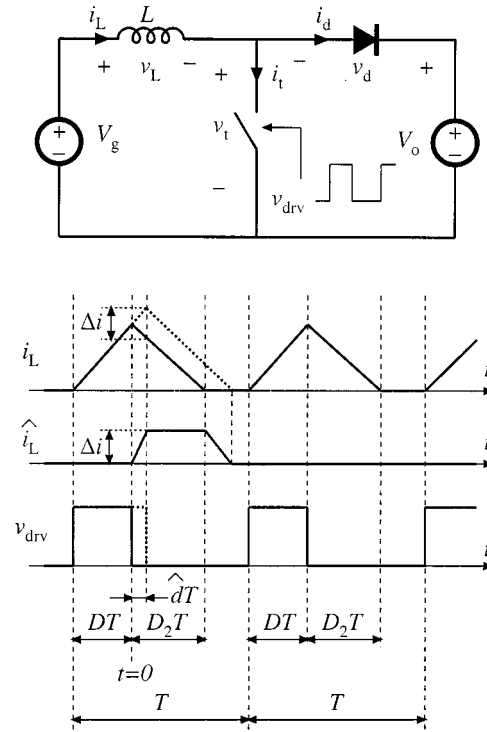


Fig. 1. Simple converter example used to introduce the impulse-response based small-signal analysis method, together with typical steady-state and transient waveforms. Parameters are: $L = 100 \mu\text{H}$, $V_g = 12 \text{ V}$, $V_o = 34 \text{ V}$, $D = 0.6$, $D_2 = 0.327$, $f_s = 1/T = 25 \text{ kHz}$.

The control-to-output “transfer function” is then

$$G_c(s) = \frac{\hat{i}_L(s)}{T\hat{d}} = \frac{V_o}{Lf_s} \frac{1 - e^{-sD_2T}}{sT} \quad (2)$$

where $f_s = 1/T$ is the switching frequency. The corresponding magnitude $\|G_c(j\omega)\|$ and phase $\angle G_c(j\omega)$ responses are shown in Fig. 2(a). The result (2) reveals that the high-frequency dynamics of DCM converters are directly related to sampling of the control input, and to the delayed response of the inductor current. These effects can only approximately be described by a continuous-time model.

From (2), an approximate continuous-time model can be obtained directly using Padé expansion:¹

$$G_c(s) \approx G_c(0) \frac{1}{1 + s/\omega_p} \quad (3)$$

where the low-frequency gain $G_c(0)$ is

$$G_c(0) = \frac{V_o D_2}{Lf_s} \quad (4)$$

and the pole frequency is given by

$$f_p = \frac{f_s}{\pi} \frac{1}{D_2}. \quad (5)$$

As shown in Fig. 2(b), the magnitude and phase responses corresponding to (3) agree very well with the exact responses obtained from (2) in a wide range of frequencies. Although the result (5) was derived for a specific converter configuration shown in Fig. 1, using the unified analysis approach from [16], it can be shown that the same expression for the high-frequency pole holds for all basic PWM converters operating in DCM. It is interesting to note that the pole frequency predicted by (5) is al-

¹The first-order Padé expansion is $e^{-sD_2T} \approx (1 - sD_2T/2)/(1 + sD_2T/2)$

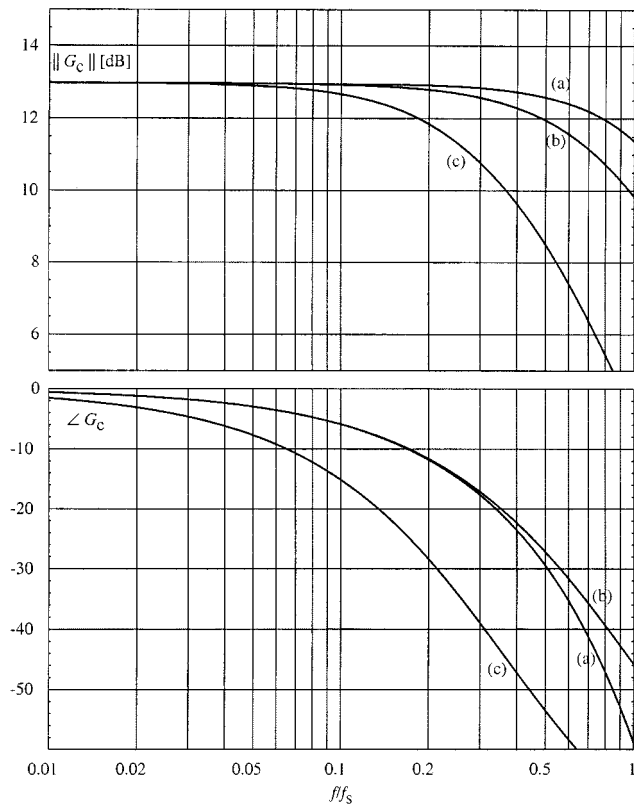


Fig. 2. Comparison of magnitude and phase responses of $G_c = \hat{i}_L / \hat{d}$ in the converter of Fig. 1 as functions of the normalized frequency f/f_s , obtained using the result of (a) impulse-response-based analysis (2); (b) approximate continuous-time model (3)–(5), and (c) full-order approximate continuous-time models [15], [16]. The responses predicted by corrected average models [19], [20] are the same as (b).

ways greater than f_s/π , and that it is inversely proportional to the length of the interval when the diode is conducting. This is not surprising because D_2T is exactly the length of the converter impulse response, i.e., the length of the delayed response in the inductor current.

The results (2) and (3)–(5) can be now be used to examine and compare several existing approaches to modeling converters in DCM.

In the basic sampled-data model (which was applied in [6], and elsewhere), samples of the state variables at the sampling instant in the k th switching period are related to the samples of the control inputs in the same switching period and the samples of the state variables in the previous switching period. The time-domain responses between the sampling instants are ignored. In the example of Fig. 2, the basic sample-data model is

$$\hat{i}_{Lk} = \frac{V_o}{Lf_s} \hat{d}_k. \quad (6)$$

The corresponding frequency response is constant at all frequencies, in contrast to the results shown in Fig. 2. This example illustrates the importance of taking into account not only sampling of the control inputs but also the *continuous-time* nature of the converter outputs, i.e., the responses of the converter state variables *between* the samples. Limitations of basic sampled-data models in predicting small-signal frequency responses have been pointed out in [4] and [17].

Averaging of the converter waveforms, usually performed over a switching period, yields approximate, continuous-time models where some of the sampling effects are ignored. In the basic reduced-order model [14], the inductor dynamics are neglected, and the model results in $G_c = V_o D_2 / L f_s = \text{const.}$ at all frequencies. This value is equal to the low-frequency gain $G_c(0)$ given by (4). However, the high-frequency pole and the phase lag, which can be significant even at relatively low frequencies, are not predicted.

The inductor current dynamics are included in the full-order averaged models for converters operating in DCM [15], [16]. In one form of the full-order model, the switching devices are grouped into a switch network and averaging over a switching period² is used to determine average terminal voltages/currents of the switch network.

In the example of Fig. 1, we have for voltages

$$\langle v_L \rangle_T = dV_g - d_2(V_o - V_g) = 0, \quad (7)$$

$$\langle v_t \rangle_T = d_2V_o + (1 - d - d_2)V_g, \quad (8)$$

$$\langle v_d \rangle_T = dV_o + (1 - d - d_2)(V_o - V_g) \quad (9)$$

and for currents

$$\langle i_L \rangle_T = \frac{V_g}{2Lf_s} d(d + d_2) \quad (10)$$

$$\langle i_t \rangle_T = \frac{V_g}{2Lf_s} d^2 \quad (11)$$

$$\langle i_d \rangle_T = \frac{V_g}{2Lf_s} dd_2 \quad (12)$$

(7)–(9) give

$$\langle v_d \rangle_T = \frac{d}{d_2} \langle v_t \rangle_T \quad (13)$$

while (10)–(12) result in

$$\langle i_t \rangle_T = \frac{d}{d_2} \langle i_d \rangle_T. \quad (14)$$

The relations (13) and (14) correspond to the large-signal averaged switch model shown in Fig. 3(a). In the averaged switch model, the switches are replaced by controlled sources that depend on the control input (duty ratio d) and the average terminal voltages/currents of the switch network. In the model of Fig. 3, the length d_2T of the interval when the diode is conducting is found from (10) where V_g is eliminated using (7)

$$d_2 = \frac{2Lf_s \langle i_L \rangle_T}{V_o d}. \quad (15)$$

The averaged-switch model of Fig. 3(a) is identical to the PWM switch model described in [15], and is equivalent to the models based on the equivalent duty ratio [16], or the loss-free resistor [1, ch. 10]. These full-order models have been successfully used in practice, although some inconsistencies between model assumptions, predictions and experimental results were noted in [16].

²Average of a variable $x(t)$ over a switching period is: $\langle x \rangle_T = (1/T) \int_0^T x(t) dt$.

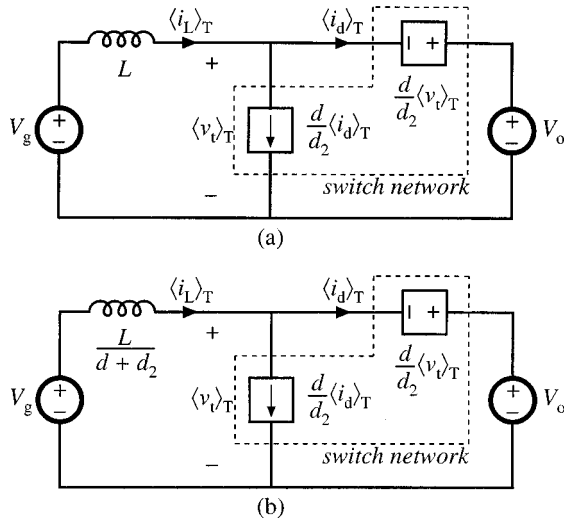


Fig. 3. Large-signal averaged switch models for the converter example of Fig. 1: (a) full-order model with $d_2 = 2Lf_s \langle i_L \rangle_T / (V_o d)$ [15], [16] and (b) corrected full-order model with $d_2 = 2Lf_s \langle i_L \rangle_T / (V_g d) - d$ [19], [20].

Perturbation of the model in Fig. 3(a) results in single-pole small-signal response $G_c(s)$ where $G_c(0)$ is identical to the gain given by (4), but the pole frequency is

$$f_p = \frac{f_s}{\pi} \frac{1}{(D + D_2)^2}. \quad (16)$$

Note that the predicted pole frequency is different from (5). The predicted magnitude and phase responses are shown in Fig. 2 for comparison with the responses obtained from (2) and (3)–(5). In this example, the full-order, continuous-time models [15], [16] clearly over-estimate the phase lag and the drop in magnitude introduced by the inductor dynamics.

The errors in the predictions of the full-order models can be traced back to the relation (7) used to derive the voltage relation (13) and the length $d_2 T$ of the interval when the diode is conducting given by (15). Since the inductor current starts from zero, and it returns to zero in each switching period, the average inductor voltage, *computed over one switching period* is indeed equal to zero. However, in the averaged, continuous-time model, the existence of inductor dynamics implies that the voltage across the inductor cannot always be zero. This “averaging paradox” has been discussed in [18], where it was concluded that averaging over a switching period may result in modeling errors because of violations of the Nyquist Sampling Theorem.

More recently, DCM models were proposed where the relation (7) is *not used* and the length of the interval $d_2 T$ is computed directly from (10) [19]–[21]

$$d_2 = \frac{2Lf_s \langle i_L \rangle_T}{dV_g} - d. \quad (17)$$

In addition, the voltage source $\langle v_d \rangle_T$ replacing the diode in the averaged-switch model is computed directly from (9). Notice that without (7) it is no longer possible to eliminate V_g and express the sources in the averaged-switch model only in terms of the averaged terminal voltages/currents of the switch network. This is why the averaged-switch models described in [19], [21]

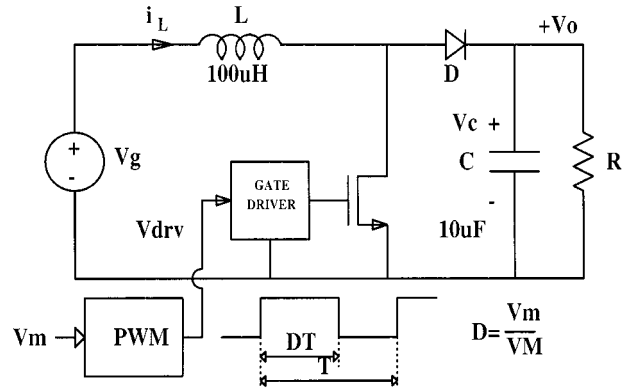


Fig. 4. Boost converter example operating in DCM: switching frequency $f_s = 1/T = 25$ kHz, dc output voltage $V_o = 33.6$ V, amplitude of the saw-tooth waveform in the pulse width modulation (PWM) $V_M = 5$ V, input to the PWM $V_m = 3$ V, duty ratio $D = V_m/V_M = 0.6$, load resistance $R = 67.5 \Omega$.

also include the inductor in the switch network. It is interesting to note that the corrected averaged-switch model can retain the form shown in Fig. 3(a) if we use (17) and allow the apparent inductance value to vary with operating conditions, as shown in Fig. 3(b).

Perturbation of the corrected full-order averaged-switch model gives a single-pole response, where the low-frequency gain and the pole frequency are *identical* to the values obtained by Padé expansion of the exact response (2) we found by evaluating the converter impulse response. Thus, the exact impulse-response based method, which takes into account sampling and delay effects, directly validates the corrected average modeling approach. A more detailed description of the corrected full-order model can be found in [20], [21].

III. SMALL-SIGNAL FREQUENCY-DOMAIN ANALYSIS BASED ON THE CONVERTER IMPULSE-RESPONSE

In the example of Fig. 1, evaluation of the frequency response from the system’s time-domain impulse response was simple and easy because the impulse response is of finite duration $D_2 T$. In general, this is not the case. Nevertheless, we will show that the same approach can be applied in general, based on the time-domain responses evaluated over several switching cycles only.

In the derivation that follows, we assume that the system is operated in steady-state for $t \leq 0$, and that a small perturbation Δu is added to the steady-state control input U during the switching period $0 \leq t \leq T$.

The boost converter in Fig. 4, and the waveforms of Fig. 5 are used to illustrate the discussion. In this example, the control input u is the input voltage v_m to the pulse-width modulator. During the initial switching period $0 \leq t \leq T$, the control input is perturbed, $v_m = V_m + \Delta v_m$. As a result, the duty ratio in this interval is slightly greater than in steady state and the corresponding perturbations can be observed in the state variables $\mathbf{x}^T(t) = [v_c(t) \ i_L(t)]$ in Fig. 5.

In general, the vector of small-signal perturbations of the state variables with respect to the steady-state trajectories $\mathbf{X}(t)$ is denoted by

$$\hat{\mathbf{x}}(t) = \mathbf{x}(t) - \mathbf{X}(t). \quad (18)$$

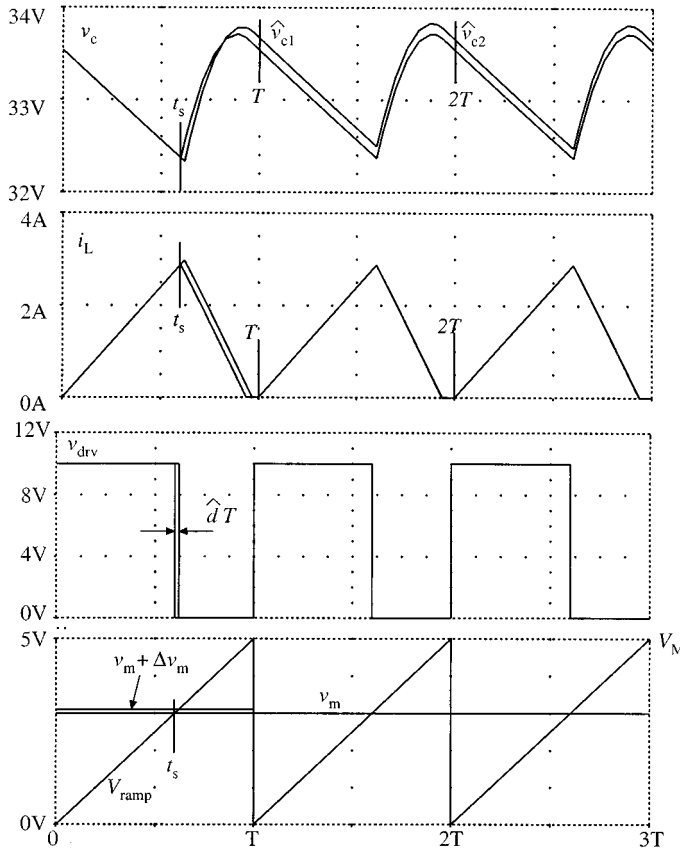


Fig. 5. Steady-state and transient simulation waveforms that illustrate impulse response of the capacitor voltage and the inductor current in the boost converter of Fig. 4.

We seek the Laplace transform of the perturbed state variables

$$\hat{\mathbf{X}}(s) = \mathcal{L}[\hat{\mathbf{x}}(t)] = \int_0^{\infty} \hat{\mathbf{x}}(t)e^{-st} dt. \quad (19)$$

First, the switching period $0 \leq t \leq T$, when the control input is perturbed, is evaluated

$$\hat{\mathbf{X}}(s) = \int_0^T \hat{\mathbf{x}}(t)e^{-st} dt + \int_T^{\infty} \hat{\mathbf{x}}(t)e^{-st} dt \quad (20)$$

$$= \hat{\mathbf{X}}_o(s) + \sum_{k=1}^{k \rightarrow \infty} \int_{kT}^{(k+1)T} \hat{\mathbf{x}}(t)e^{-st} dt \quad (21)$$

where

$$\hat{\mathbf{X}}_o(s) = \int_0^T \hat{\mathbf{x}}(t)e^{-st} dt \quad (22)$$

is the result of evaluating the impulse response over the first switching period, from $t = 0$ to $t = T$. Next, we note that the response in the k th switching period, $kT \leq t \leq (k+1)T$ can be written as

$$\hat{\mathbf{x}}(t) = \Phi(t - kT)\hat{\mathbf{x}}_k \quad (23)$$

where $\hat{\mathbf{x}}_k$ is the vector of perturbed state variables sampled at the beginning of the k th switching period, and $\Phi(t)$ is the transition matrix. So

$$\hat{\mathbf{X}}(s) = \hat{\mathbf{X}}_o(s) + \sum_{k=1}^{k \rightarrow \infty} \int_{kT}^{(k+1)T} \Phi(t - kT)\hat{\mathbf{x}}_k e^{-st} dt. \quad (24)$$

By change of variables $\tau = t - kT$, using

$$\hat{\mathbf{x}}_{k+1} = \Phi(T)\hat{\mathbf{x}}_k = \Phi_T \hat{\mathbf{x}}_k \quad (25)$$

and by changing the order of integration and summation, we have

$$\begin{aligned} \hat{\mathbf{X}}(s) &= \hat{\mathbf{X}}_o(s) + \sum_{k=1}^{k \rightarrow \infty} \int_{kT}^{(k+1)T} \Phi(t - kT)\hat{\mathbf{x}}_k e^{-st} dt \\ &= \hat{\mathbf{X}}_o(s) + \left(\int_0^T \Phi(\tau)e^{-s\tau} d\tau \right) \\ &\quad \cdot \left(\sum_{k=1}^{k \rightarrow \infty} \Phi_T^{k-1} e^{-skT} \right) \hat{\mathbf{x}}_1 \\ &= \hat{\mathbf{X}}_o(s) + \Phi(s) \left(\sum_{k=1}^{k \rightarrow \infty} \Phi_T^{k-1} e^{-skT} \right) \hat{\mathbf{x}}_1. \end{aligned} \quad (26)$$

Here

$$\Phi(s) = \int_0^T \Phi(\tau)e^{-s\tau} d\tau \quad (27)$$

is the *equivalent hold* first introduced in [4]. This part of the response, which is due to evaluating the converter time-domain responses *between the samples*, is often missing in various sampled-data models.

The summation over k can be performed as follows:³

$$\begin{aligned} \sum_{k=1}^{k \rightarrow \infty} \Phi_T^{k-1} e^{-skT} &= e^{-sT} \sum_{k=0}^{k \rightarrow \infty} (\Phi_T e^{-sT})^k \\ &= e^{-sT} (I - \Phi_T e^{-sT})^{-1} \\ &= (e^{sT} I - \Phi_T)^{-1} \end{aligned} \quad (28)$$

which gives the final result

$$\hat{\mathbf{X}}(s) = \hat{\mathbf{X}}_o(s) + \Phi(s) (e^{sT} I - \Phi_T)^{-1} \hat{\mathbf{x}}_1. \quad (29)$$

Using (29), the control-to-state responses $\mathbf{H}(s) = \hat{\mathbf{x}}/\hat{u}$ can be obtained as

$$\mathbf{H}(s) = \frac{1}{T\Delta u} \hat{\mathbf{X}}(s)e^{st_s} \quad (30)$$

where sampling of the control input gives the scale factor $1/T$ (see, for example, [22, Sect. 8.1]). Since sampling of the control input and the corresponding changes in the state variables occur at $t = t_s$ after the beginning of the initial switching period at $t = 0$, the shift in time by t_s is accounted for by the factor e^{st_s} .

If the response of outputs \mathbf{y} other than state variables \mathbf{x} is desired, it is necessary to replace $\hat{\mathbf{X}}_o(s)$ and $\Phi(s)$ with the responses obtained by evaluating the time-domain transients of the specified outputs. From the response in the initial switching period

$$\hat{\mathbf{Y}}_o(s) = \int_0^T \hat{\mathbf{y}}(t)e^{-st} dt. \quad (31)$$

As in (23), the output response in the k th switching period, $kT \leq t \leq (k+1)T$ can be written as

$$\hat{\mathbf{y}}(t) = \Gamma(t - kT)\hat{\mathbf{x}}_k \quad (32)$$

³Assuming that the sum is convergent, we make use of the matrix identity $(I - \mathbf{A})^{-1} = I + \mathbf{A} + \mathbf{A}^2 + \dots$, where $\mathbf{A} = \Phi_T e^{-sT}$

and the equivalent hold for the selected outputs becomes

$$\mathbf{\Gamma}(s) = \int_0^T \mathbf{\Gamma}(\tau) e^{-s\tau} d\tau. \quad (33)$$

In general, in a state-space description of a system, the outputs are functions of states and inputs. Except during the initial switching period which is evaluated in (31), the input perturbation is zero, so that the relation (32) which gives outputs in terms of states only holds true in general for our purposes.

Finally

$$\hat{\mathbf{Y}}(s) = \hat{\mathbf{Y}}_o(s) + \mathbf{\Gamma}(s) (e^{sT} \mathbf{I} - \mathbf{\Phi}_T)^{-1} \hat{\mathbf{x}}_1 \quad (34)$$

and the desired control-to-output responses $\mathbf{G}(s) = \hat{\mathbf{y}}/\hat{u}$ are obtained as

$$\mathbf{G}(s) = \frac{1}{T\Delta u} \hat{\mathbf{Y}}(s) e^{st_s}. \quad (35)$$

The impulse-response-based model (29), (30), (34), and (35) is in fact equivalent to the exact small-signal model described in [4] for piecewise-linear switched systems, but the formulation is changed to accommodate our objective of using a general-purpose simulator to numerically evaluate the required responses. In addition, since the responses are obtained using numerical time-domain simulation, the converter model need not be piecewise linear, and arbitrarily complex, nonlinear device models supported by the simulator can be applied.

IV. IMPLEMENTATION USING A GENERAL-PURPOSE SIMULATION TOOL

In this section, we describe how the model based on the results of Section III can be implemented using a general-purpose time-domain simulation tool. The algorithm is described in steps:

- 1) Find steady-state initial conditions $\mathbf{X}(0)$ for the state variables. Here we use the methods for accelerated convergence to steady state described in [11]. In general, small-signal responses can also be found around arbitrary, not necessarily steady-state, large-signal trajectories.
- 2) Run a transient simulation over the initial switching period with an input u perturbed, $u = U + \Delta u$. Results of this simulation are used to numerically obtain $\hat{\mathbf{X}}_o(s)$, $\hat{\mathbf{Y}}_o(s)$, and the vector of perturbed state variables $\hat{\mathbf{x}}_1$ at the end of the period.
- 3) Run n transient simulations ($1 \leq j \leq n$, where n is the number of state variables) over a switching period with the steady state input U and a perturbed initial condition $x_j(0) = X_j(0) + \Delta x_j$ for the j th state variable. The j th simulation is used to compute the j th column of $\mathbf{\Phi}(s)$ and $\mathbf{\Gamma}(s)$, and to determine the j th column of $\mathbf{\Phi}_T$ as $\hat{\mathbf{x}}(T)/\Delta x_j$.
- 4) The results of Steps 2 and 3 are combined to obtain $\mathbf{H}(s)$ given by (30) and $\mathbf{G}(s)$ given by (35). Magnitude and phase frequency responses can then be plotted for the output variables of interest.

Steps 1–4 have been completely automated using the setup shown in Fig. 6. The implementation setup is similar to the setups reported in [6], [10]: a front-end program manipulates the data and controls a general-purpose simulator which is used to generate time-domain responses. Two simulators are supported:

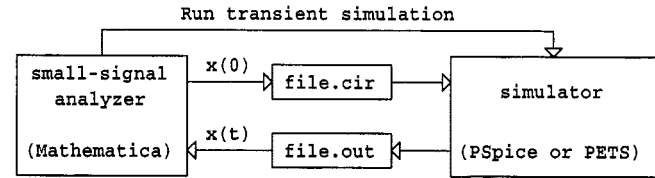


Fig. 6. Implementation setup: *Mathematica* updates the circuit netlist file with initial conditions $\mathbf{x}(0)$, and launches the simulator (PSPice or PETS) to obtain the response $\mathbf{x}(t)$ over the switching period. The response data are used to generate small-signal frequency responses in *Mathematica*.

PSPice and PETS [12]. The functions of updating the inputs and initial conditions in the circuit netlist file, launching the simulator, as well as performing all manipulations on the data collected from simulation have been written in *Mathematica* [13]. In finding the transfer functions $\mathbf{H}(s)$, $\mathbf{G}(s)$, symbolic computation capabilities of *Mathematica* are used to keep $s = j\omega$ as a variable. As a result, *only* $n + 1$ simulation runs over the switching period and one symbolic matrix inversion are needed to obtain and evaluate the frequency responses at all signal frequencies.

V. APPLICATION EXAMPLES

The method described in Sections III and IV is general in the sense that control-to-output frequency responses can be generated for any circuit model supported by the selected time-domain simulator. Practical applications can be found in investigation of frequency responses of systems where analytical models are unknown or where existing analytical techniques are difficult to apply, as well as for general computer-aided design verification purposes when second-order effects may be included. Two examples are included in this section: a DCM boost converter, and a multiple-output flyback converter. Another application example was reported in [24].

A. Boost Converter in Discontinuous Conduction Mode

The first example that we consider is the boost converter shown in Fig. 4. The converter operates in discontinuous conduction mode. This example is used to validate numerical implementation of the method and to provide another verification of our conclusions regarding various averaged models for DCM.

The results obtained using the automated impulse-response-based method are shown in Fig. 7:

- 1) together with experimental data and predictions of the reduced-order [14];
- 2) the full-order [15], [16];
- 3) the corrected full-order [19]–[21];
- 4) approximate continuous-time analytical models.

The automated small-signal analysis method (using PETS to generate time-domain responses) gives results in excellent agreement with both experimental data and with the responses predicted by the corrected full-order model.

B. Dynamics of a Multiple-Output Flyback Converter

The second example is motivated by an application where appropriate analytical models are not readily available. The example is an experimental three-output, 100 kHz flyback con-

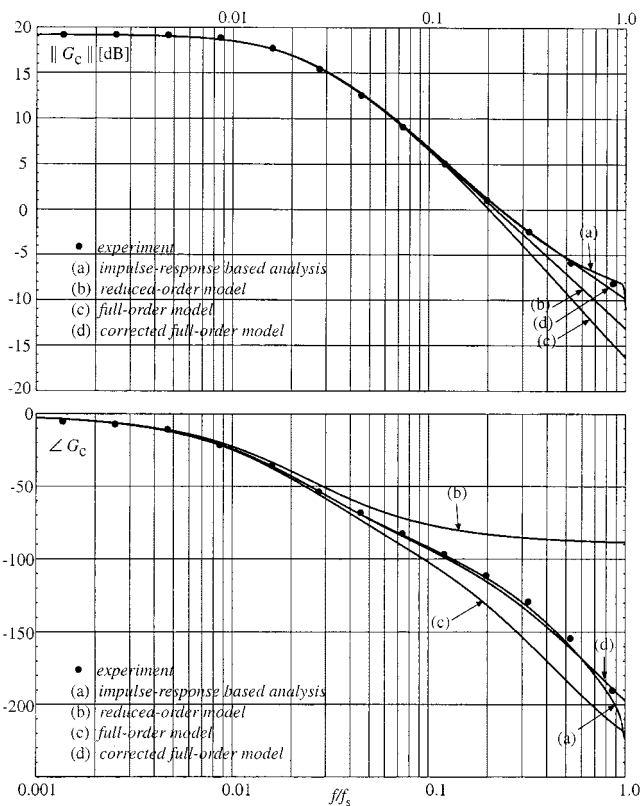


Fig. 7. Magnitude and phase responses of the control-to-output transfer function \hat{v}_c/\hat{v}_m as functions of the normalized signal frequency f/f_s for the boost converter in Fig. 4.

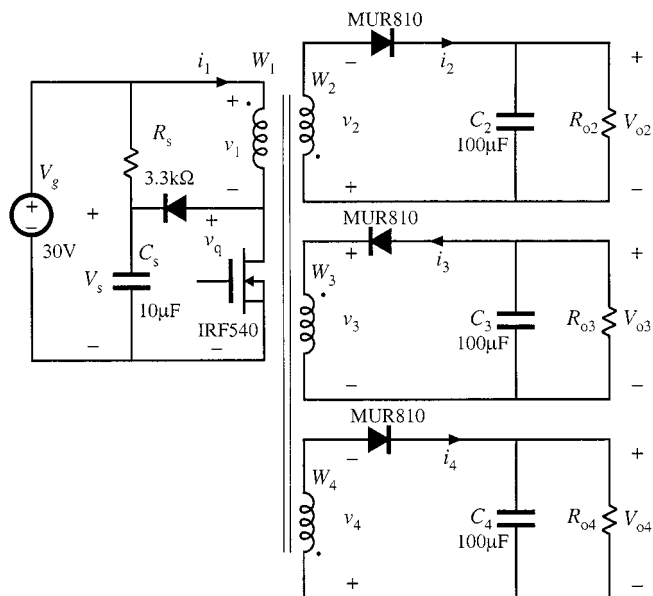


Fig. 8. Experimental three-output flyback converter.

verter shown in Fig. 8. The input is $V_g = 30$ V, and the nominal outputs are: $V_{o2} = +12$ V, $V_{o3} = -12$ V, $V_{o4} = 3.3$ V. The 3.3 V (winding W_4) output is taken to be the main output that would be regulated by a feedback loop. The transformer was constructed on a ferrite EC41-3C80 core, having a 0.5 mm air gap in each leg. The winding configuration is shown in Fig. 9.

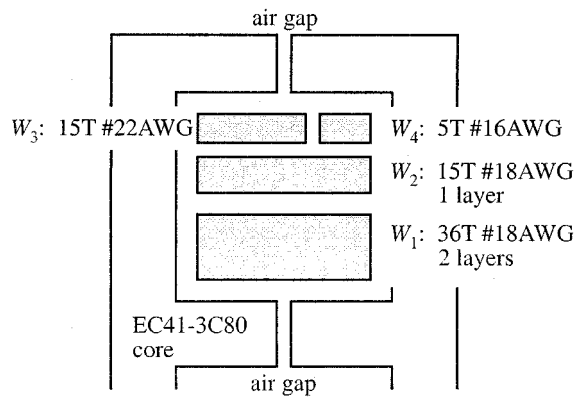


Fig. 9. Winding geometry of the flyback transformer.

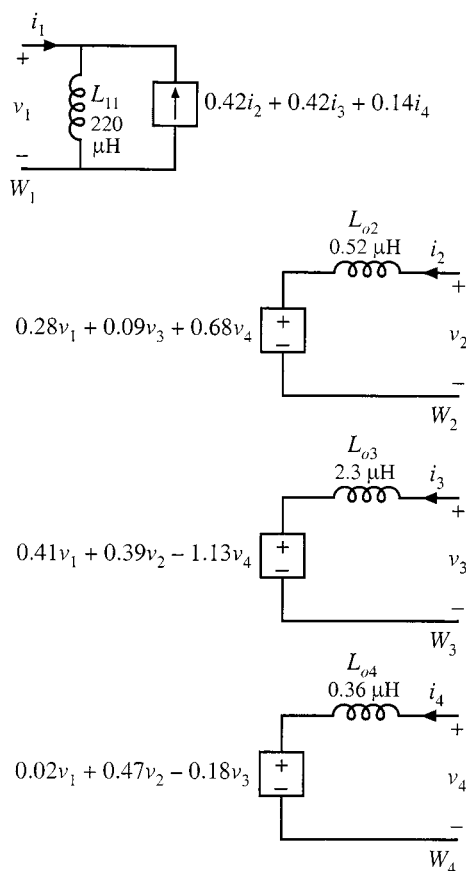


Fig. 10. N-port model of the flyback transformer.

Magnetics models suitable for analysis of multiple-output converters were discussed in [23]. In particular, a general model that captures all details of magnetic couplings, and is particularly well suited for simulation, is the N-port model shown in Fig. 10, with the parameters shown for the flyback transformer in Fig. 9. All parameters in this model are obtained experimentally as described in [23].

In a multiple-output flyback converter, leakage inductances, which are usually considered second-order effects, very strongly affect even the steady-state solution. The converter can operate in a number of different modes, depending on the values of the load currents, and transformer magnetizing and leakage inductances.

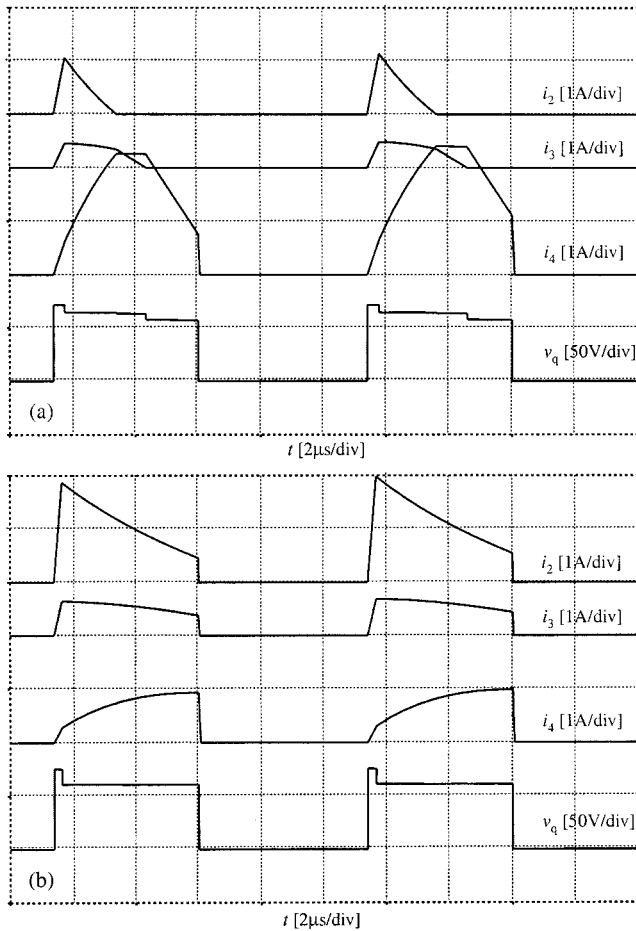


Fig. 11. Waveforms in the flyback converter at two operating points: (a) $D = 0.52$, $V_{o2} = 13.5$ V, $V_{o3} = 14.2$ V, $V_{o4} = 3.4$ V, $V_s = 71$ V, $R_{o2} = 150$ Ω , $R_{o3} = 170$ Ω , $R_{o4} = 5$ Ω and (b) $D = 0.52$, $V_{o2} = 12.1$ V, $V_{o3} = 12.3$ V, $V_{o4} = 3.4$ V, $V_s = 75$ V, $R_{o2} = 25$ Ω , $R_{o3} = 50$ Ω , $R_{o4} = 10$ Ω .

tances. Because of the complex behavior, and the lack of suitable magnetics models in the past, very few analytical results are now available to predict steady-state or dynamic responses of multiple-output flyback converters.

Here, the objective was to find the control-to-main output response \hat{v}_{o4}/\hat{d} . Of particular interest is the substantial change that occurs in the control-to main output response when auxiliary outputs change between continuous conduction and discontinuous conduction mode. The magnitude and phase responses were measured at two different operating points: a) when both auxiliary outputs (windings W_2 , W_3) operated in discontinuous conduction mode, and b) with both auxiliary outputs operated in continuous conduction mode. In both cases, the main output (winding W_4) operated in continuous conduction mode. The operating points and the corresponding steady-state waveforms obtained by PETS simulation are shown in Fig. 11. In the simulations, semiconductor conduction losses were modeled, the transformer model was as shown in Fig. 10, while other nonidealities such as capacitor ESR, switching loss, and transformer losses, were neglected.

Notice that the three-output flyback converter is relatively complex, eight-order system. Nevertheless, the automated steady-state solver [11] and the impulse-response based

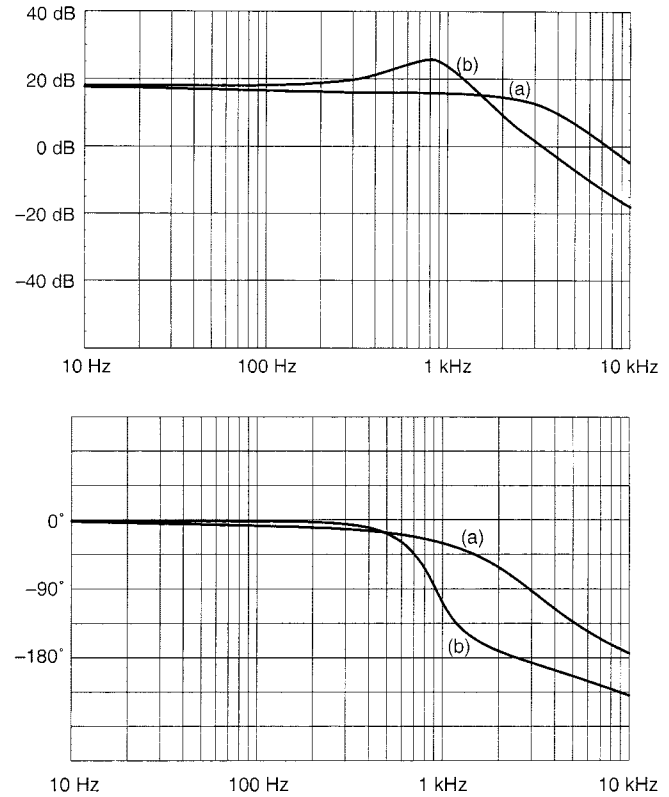


Fig. 12. Magnitude and phase control-to-main output responses \hat{v}_{o4}/\hat{d} obtained using the automated impulse-response based analysis, with the main W_4 output in CCM and (a) with W_2 and W_3 outputs in DCM and (b) with W_2 and W_3 outputs in CCM.

REF LEVEL	/DIV
0.000dB	10.000dB
-90.000deg	45.000deg

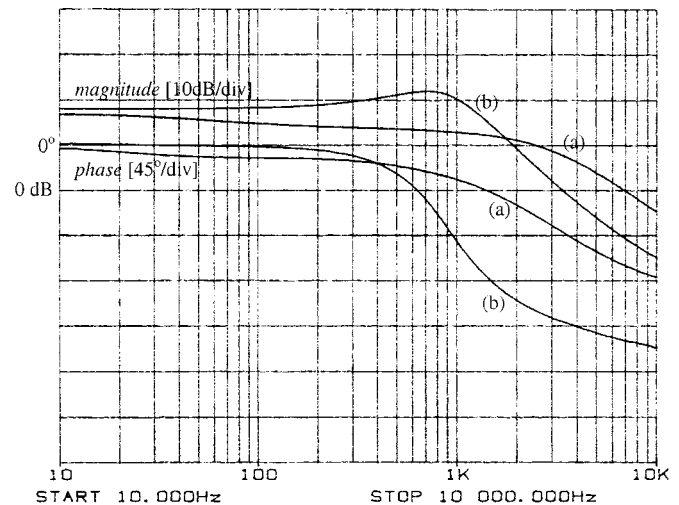


Fig. 13. Measured magnitude and phase control-to-main output responses \hat{v}_{o4}/\hat{d} with the main W_4 output in CCM and (a) with W_2 and W_3 outputs in DCM and (b) with W_2 and W_3 outputs in CCM.

small-signal analysis method implemented as described in Section IV converged quickly and easily. Predicted magnitude and phase responses at the two operating points are illustrated in Fig. 12. The measured small-signal responses are given in

Fig. 13. The agreement is quite good. It is interesting to note that the change of operating mode on the auxiliary outputs has quite noticeable effect on the main-output current waveform, and also on small-signal control-to-main output frequency response.

VI. CONCLUSIONS

The paper describes a method for automated small-signal frequency response analysis based on the converter impulse response obtained using a general purpose simulation tool. In our implementation, two simulation tools are supported: PSpice and PETS, while the functions of launching the simulator, collecting and manipulating the data have been written in *Mathematica*.

The main advantage of the proposed method as a design verification tool is that frequency responses can be generated efficiently and accurately for any converter configuration and any model complexity supported by the general-purpose simulator. Selected application examples are included to show good correlation between the generated responses and experimental data, as well as to compare the results with predictions of approximate continuous-time models. In particular, the impulse-response based method is applied to investigate high-frequency dynamics of PWM converters operating in discontinuous conduction mode, and the results are used to evaluate and compare several existing analytical modeling approaches.

REFERENCES

- [1] R. W. Erickson, *Fundamentals of Power Electronics*. London, U.K.: Chapman and Hall, 1997.
- [2] A. Kislovski, R. Redl, and N. Sokal, *Dynamic Analysis of Switching-Mode dc/dc Converters*. New York: Van Nostrand Reinhold, 1994.
- [3] J. G. Kassakian, M. F. Schlecht, and G. C. Verghese, *Principles of Power Electronics*. Reading, MA: Addison-Wesley, 1991.
- [4] B. Y. Lau and R. D. Middlebrook, "Small-signal frequency response theory for piecewise-constant two-switched-network dc-to-dc converter systems," in *Proc. IEEE PESC 86*, 1986, pp. 186–200.
- [5] R. Tymerski, "Application of time varying transfer function for exact small-signal analysis," in *Proc. IEEE PESC'91*, 1991, pp. 80–87.
- [6] P. Maranesi, "PWM converter characterization in the frequency domain through fast time-domain computer simulation," in *Proc. 2nd Workshop Comput. Power Electron.*, 1990.
- [7] J. Groves, "Small-signal analysis using harmonic balance methods," in *Proc. IEEE PESC'91*, 1991, pp. 74–79.
- [8] R. C. Wong and J. Groves, "An automated small-signal frequency-domain analyzer for general periodic-operating systems as obtained via time-domain simulation," in *Proc. IEEE PESC'95*, 1995, pp. 801–808.
- [9] P. Huynh and B. H. Cho, "Empirical small-signal modeling of switching converters using PSpice," in *Proc. IEEE PESC'95*, 1995, pp. 809–815.

- [10] D. C. Hamil, "Improved time-domain simulation of resonant and other dc–dc converters," in *Proc. 2nd Workshop Comput. Power Electron.*, 1990.
- [11] D. Maksimović, "Automated steady-state analysis of switching power converters using a general-purpose simulation tool," in *Proc. IEEE PESC'97*, 1997.
- [12] P. Pejović and D. Maksimović, "PETS—A simulation tool for power electronics," in *Proc. 1996 IEEE Workshop Comput. Power Electron.*, 1996.
- [13] S. Wolfram, *The Mathematica Book*, 3rd ed. Cambridge, U.K.: Wolfram Media and Cambridge Univ. Press, 1996.
- [14] S. Čuk and R. D. Middlebrook, "A general unified approach to modeling dc-to-dc converters in discontinuous conduction mode," in *Proc. IEEE PESC'77*, 1977, pp. 36–57.
- [15] V. Vorperian, "Simplified analysis of PWM converters using the model of the PWM switch—Parts I and II," *IEEE Trans. Aerosp. Electron. Syst.*, vol. 26, pp. 490–505, May 1990.
- [16] D. Maksimović and S. Čuk, "A unified analysis of PWM converters in discontinuous modes," *IEEE Trans. Power Electron.*, vol. 6, July 1991.
- [17] R. Tymerski, "On the efficacy of sampled data modeling of switched networks," in *Proc. 5th IEEE Workshop Comput. Power Electron.*, 1996, pp. 14–17.
- [18] S. Ben-Yaakov, D. Wulich, and W. M. Polivka, "Resolution of an averaging paradox in the analysis of switched-mode dc–dc converters," *IEEE Trans. Aerosp. Electron. Syst.*, vol. 30, pp. 626–632, Apr. 1994.
- [19] S. Ben-Yaakov and D. Adar, "Average models as tools for studying the dynamics of switch mode dc–dc converters," in *Proc. IEEE PESC 94*, 1994, pp. 1369–1376.
- [20] J. Sun, D. M. Mitchell, M. Greuel, P. T. Krein, and R. M. Bass, "Averaged modeling of PWM converters in discontinuous conduction mode: A reexamination," in *Proc. IEEE PESC'98*, 1998, pp. 615–622.
- [21] —, "Averaged models for PWM converters in discontinuous conduction mode," in *Proc. HFPC'98*, 1998.
- [22] A. V. Oppenheim and A. S. Willsky, *Signals and Systems*. Englewood Cliffs, NJ: Prentice-Hall, 1983.
- [23] R. W. Erickson and D. Maksimović, "A multiple-winding magnetics model having directly measurable parameters," in *Proc. IEEE PESC'98*, 1998.
- [24] D. Maksimović, "Automated small-signal analysis of switching converters using a general-purpose time-domain simulator," in *Proc. IEEE APEC'98*, 1998.



Dragan Maksimović (M'89) was born in Belgrade, Yugoslavia, on July 15, 1961. He received the B.S. and M.S. degrees in electrical engineering from the University of Belgrade, in 1984 and 1986, respectively, and the Ph.D. degree from the California Institute of Technology, Pasadena, in 1989.

From 1989 to 1992, he was with the University of Belgrade. Since 1992, he has been with the Department of Electrical and Computer Engineering, University of Colorado, Boulder, where he is currently an Associate Professor and Co-Director of the Colorado

Power Electronics Center (CoPEC). His current research interests include simulation and control techniques, low-harmonic rectifiers, and power electronics for low-power, portable systems.

Dr. Maksimović received the NSF CAREER Award and a Power Electronics Society Transactions Prize Paper Award in 1997.